IOP PUBLISHING METROLOGIA
Metrologia **47** (2010) 33–46 doi:10.1088/0026-1394/47/1/005

Effective emissivity of a cylindrical cavity with an inclined bottom: II. Non-isothermal cavity

Alexander V Prokhorov and Leonard M Hanssen

National Institute of Standards and Technology, 100 Bureau Drive, Gaithersburg, MD 20899, USA

E-mail: leonard.hanssen@nist.gov

Received 20 July 2009, in final form 23 November 2009
Published 16 December 2009
Online at stacks.iop.org/Met/47/33

Abstract
An algorithm of the Monte Carlo method applied to the computation of the spectral and total effective emissivity of a specular–diffuse, non-isothermal blackbody cavity formed by a cylindrical tube and a flat inclined bottom is described. The effect of cavity wall temperature non-uniformity on the cavity radiation characteristics is studied for various combinations of the affecting parameters.

1. Introduction

In the first part of this work [1], we described the application of the Monte Carlo method to modelling of the effective emissivity of an isothermal, specular–diffuse cylindrical cavity with an inclined bottom. Now we expand the analysis on such a cavity having a non-isothermal internal surface.

The effective emissivity of a cavity depends on its geometric parameters, wall reflectance and diffusity, temperature distribution over the cavity wall as well as the conditions of observation. The isothermal approximation is very useful but not always adequate. Real cavities are non-isothermal in varying degrees. In order to recall the existing methods for the calculation of effective emissivities of isothermal and non-isothermal cavities, we refer the interested reader to the reviews [2, 3]. The majority of these methods were developed for axisymmetric cavities with diffuse walls, so the most common properties of a cylindrical cavity with an inclined bottom and a non-isothermal radiating surface remain unexplored. Taking into account the large number of critical factors and the limited space available, we cannot present an analysis of all the existing dependences. It is clearly impossible to provide numerical results for effective emissivities for all possible temperature distributions, which to a great extent depend on the design and materials of a particular blackbody radiator. The scope of this paper is limited to the simple models used for temperature distributions.

2. Definition of the effective emissivities for a non-isothermal cavity

The reader is referred to the first part of this work [1] for the detailed descriptions and definitions of the various forms of effective emissivity, of which several are used in this paper. The total and spectral local, directional effective emissivities for a non-isothermal cavity are defined, as for the isothermal case, as a ratio of radiances or spectral radiances, respectively, of an infinitesimal element of a cavity wall in a given direction to the corresponding quantity of a perfect blackbody. The principal distinction from the isothermal cavity case is the fact that there is no unambiguous choice of the temperature assigned to a non-isothermal cavity to compare it with a perfect blackbody. That is why a specific temperature called the 'reference temperature', T_{ref}, is usually chosen to characterize the non-isothermal blackbody. The temperature of the bottom centre (see, for instance, [2, 4, 5]) is suitable for selection as T_{ref}.

The local, directional spectral effective emissivity for a non-isothermal cavity in a non-refractive environment can be written in the form

$$\varepsilon_{\mathrm{e}}(\lambda, \vec{\xi}, \vec{\omega}, T_{\mathrm{ref}}) = \frac{L_{\lambda}(\lambda, \vec{\xi}, \vec{\omega})}{L_{\lambda,\mathrm{bb}}(\lambda, T_{\mathrm{ref}})}, \tag{1}$$

where L_{λ} and $L_{\lambda,\mathrm{bb}}$ are, respectively, the spectral radiance of a cavity with a reference temperature T_{ref}, at a point $\vec{\xi}$, a wavelength λ and in a direction $\vec{\omega}$, and that of a

perfect blackbody, for the same temperature, wavelength and direction. The denominator in equation (1) can be computed by Planck's law:

$$L_{\lambda,\mathrm{bb}}(\lambda, T_{\mathrm{ref}}) = \frac{c_1}{\pi \cdot \lambda^5[\exp(c_2/(\lambda \cdot T_{\mathrm{ref}})) - 1]}, \qquad (2)$$

where $c_1 = 3.741\,771\,18(19) \times 10^{-16}\,\mathrm{W\,m^2}$ and $c_2 = 1.438\,775\,2(25) \times 10^{-2}\,\mathrm{m\,K}$ are the first and second radiation constants, respectively [6].

Integration over the entire spectrum gives the directional total effective emissivity as a ratio of corresponding radiances. One can write, using the Stefan–Boltzmann law,

$$\varepsilon_{\mathrm{t,e}}(\vec{\xi}, \vec{\omega}, T_{\mathrm{ref}}) = \frac{\pi L(\vec{\xi}, \vec{\omega})}{\sigma T_{\mathrm{ref}}^4}, \qquad (3)$$

where L is the radiance of a cavity wall at a point $\vec{\xi}$ in a direction $\vec{\omega}$; $\sigma = 5.670\,400(40) \times 10^{-8}\,\mathrm{W\,m^{-2}\,K^{-4}}$ is the Stefan–Boltzmann constant [6].

Since the choice of T_{ref} is arbitrary, the effective emissivity of a non-isothermal cavity is a function of this temperature. It is easy to show that

$$\varepsilon_{\mathrm{e}}(\lambda, T_{\mathrm{ref}}) = \varepsilon_{\mathrm{e}}(\lambda, T'_{\mathrm{ref}})\frac{L_{\lambda,\mathrm{bb}}(\lambda, T'_{\mathrm{ref}})}{L_{\lambda,\mathrm{bb}}(\lambda, T_{\mathrm{ref}})}$$
$$= \varepsilon_{\mathrm{e}}(\lambda, T'_{\mathrm{ref}})\frac{\exp(c_2/\lambda T'_{\mathrm{ref}}) - 1}{\exp(c_2/\lambda T_{\mathrm{ref}}) - 1} \qquad (4)$$

and

$$\varepsilon_{\mathrm{t,e}}(T_{\mathrm{ref}}) = \varepsilon_{\mathrm{t,e}}(T'_{\mathrm{ref}})\frac{L_{\mathrm{bb}}(T'_{\mathrm{ref}})}{L_{\mathrm{bb}}(T_{\mathrm{ref}})} = \varepsilon_{\mathrm{t,e}}(T'_{\mathrm{ref}})\left(\frac{T'_{\mathrm{ref}}}{T_{\mathrm{ref}}}\right)^4, \qquad (5)$$

where L_{bb} is the radiance of a perfect blackbody, T_{ref} and T'_{ref} are two arbitrarily chosen reference temperatures.

The effective emissivity of a non-isothermal cavity can be less than, equal to or greater than unity, depending on the choice of reference temperature and the actual temperature distribution. But it is clear that the choice of the reference temperature does not affect the emitted radiance and spectral radiance of a cavity.

By analogy with the first part of this work [1], it is possible to introduce the other types of effective emissivity which can be computed by averaging over the spectral, spatial and angular domains.

3. Background radiation effects

The approximation of an isothermal cavity implies a non-radiating environment. However, this assumption is valid only if the temperature of a blackbody source is much higher than that of the surrounding environment. A real ambient background always has a temperature greater than absolute zero. Therefore, it must emit thermal radiation that irradiates the aperture of a cavity. After multiple reflections inside a cavity, this radiation together with the cavity's own thermal radiation can reach the detector. This effect is especially significant for low-temperature blackbodies with moderate values of effective emissivity. Since the spectral, spatial and angular distributions of background radiation are usually unknown, the simplest case of isotropic blackbody radiation that corresponds to a background temperature T_{bg} can be considered, i.e. every point of a virtual surface subtending the cavity opening is considered as a blackbody source with the temperature T_{bg} and obeys the laws of Planck, Stefan–Boltzmann and Lambert. We assume that it is possible to neglect the radiation exchange between the cavity and the detector, and that the detector does not distort the isotropy of the background radiation.

Let us consider an isothermal cavity at a temperature T_0 with an effective emissivity ε_{e} determined for the case of a non-radiating background and some collecting geometry of the cavity radiation determined by the detection system. The effect of an isotropic background at a temperature T_{bg} can be accounted for by the equation:

$$\varepsilon'_{\mathrm{t,e}}(T_0, T_{\mathrm{bg}}) = \varepsilon_{\mathrm{e}} + (1 - \varepsilon_{\mathrm{e}})\left(\frac{T_{\mathrm{bg}}}{T_0}\right)^4 \qquad (6)$$

for the total effective emissivity and

$$\varepsilon'_{\mathrm{e}}(\lambda, T_0, T_{\mathrm{e}}) = \varepsilon_{\mathrm{e}} + (1 - \varepsilon_{\mathrm{e}})\frac{\exp(c_2/\lambda T_0) - 1}{\exp(c_2/\lambda T_{\mathrm{bg}}) - 1} \qquad (7)$$

for the spectral effective emissivity.

Note that the spectral effective emissivity becomes wavelength-dependent even for an isothermal cavity with grey internal surfaces as long as the temperatures of the cavity and the environment are different. The addends in equations (6) and (7) (correction terms for background radiation) vanish when $T_{\mathrm{bg}} \ll T_0$. For a non-isothermal cavity, due to the additivity of radiant fluxes, the correction terms for the background radiation remain the same—we only need to know the effective emissivity of an appropriate isothermal cavity determined for a non-emitting environment:

$$\varepsilon'_{\mathrm{t,e}}(T_{\mathrm{ref}}, T_{\mathrm{bg}}) = \varepsilon_{\mathrm{t,e}}(T_{\mathrm{ref}}) + (1 - \varepsilon_{\mathrm{e}})\left(\frac{T_{\mathrm{bg}}}{T_{\mathrm{ref}}}\right)^4 \qquad (8)$$

for the total effective emissivity and

$$\varepsilon'_{\mathrm{e}}(\lambda, T_{\mathrm{ref}}, T_{\mathrm{bg}}) = \varepsilon_{\lambda,\mathrm{e}}(\lambda, T_{\mathrm{ref}}) + (1 - \varepsilon_{\mathrm{e}})\frac{\exp(c_2/\lambda T_{\mathrm{ref}}) - 1}{\exp(c_2/\lambda T_{\mathrm{bg}}) - 1} \qquad (9)$$

for the spectral effective emissivity.

4. Monte Carlo ray-tracing algorithm for a non-isothermal cavity

Our algorithm employed for the numerical modelling of a non-isothermal cavity is similar to that used in the first part of this work [1] for an isothermal cavity. The backward (inverse) ray-tracing technique is also applied, i.e. every ray begins at the observation point outside the cavity, passes through its aperture and undergoes multiple reflections from the cavity's internal wall. The temperature distribution is specified by its values at the nodes of a one- or two-dimensional grid superimposed on the cavity radiating surface. We assume that there is

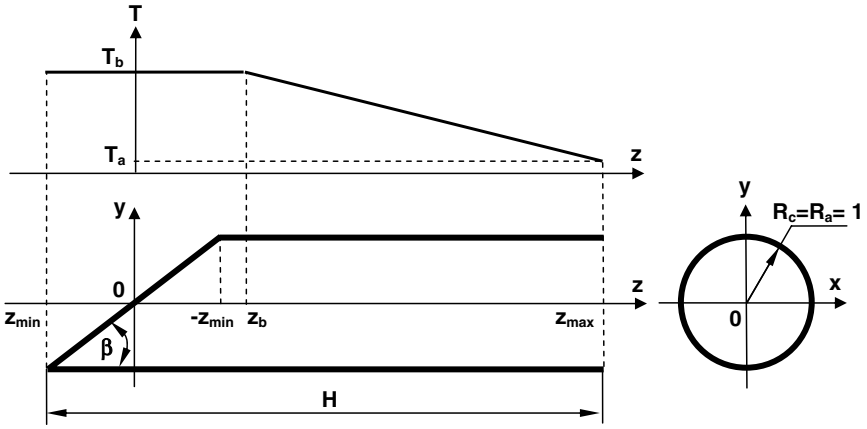

Figure 1. Model of a cavity with an inclined bottom and model of the temperature distributions used for computations.

no background radiation, i.e. $T_{\mathrm{bg}} = 0\,\mathrm{K}$ (if this is not true, corresponding corrections can be made at the post-processing stage). For simplicity, the optical properties are assumed to be spatially uniform over the cavity radiating surface.

The radiance of a ray, which is observed from outside the cavity in the forward direction is equal to

$$L = L_1 + \rho(L_2 + \rho(L_3 + \cdots + \rho L_M)) = \sum_{k=1}^{M} L_k \rho^{k-1}, \qquad (10)$$

where the index k varies from 1 to the number of reflections M in the ray trajectory, $\rho = 1 - \varepsilon_{\mathrm{t}}$ is the cavity wall reflectance, ε_{t} is its total emissivity and $L_k, k = 1, 2, \ldots, M$, are the radiance values of the thermal radiation emitted by the cavity wall at the points of successive reflections, i.e. $L_1 = \varepsilon_{\mathrm{t}}\sigma T_1^4$ corresponds to the radiation that propagates along the direction of observation and reaches the observation point directly (with no reflections), $L_2 = \varepsilon_{\mathrm{t}}\sigma T_2^4$ corresponds to the radiation that reaches the observation point after one reflection, and so forth; $T_k, k = 1, 2, \ldots, M$ are the temperatures at the corresponding points.

The analogous expression for spectral radiance is

$$L_\lambda = L_{\lambda,1} + \rho(\lambda)(L_{\lambda,2} + \rho(\lambda)(L_{\lambda,3} + \cdots + \rho(\lambda)L_{\lambda,M})) = \sum_{k=1}^{M} L_{\lambda,k}\rho^{k-1}(\lambda), \qquad (11)$$

where $\rho(\lambda) = 1 - \varepsilon(\lambda)$ is the cavity wall spectral reflectance at the wavelength λ, $\varepsilon(\lambda)$ is its spectral emissivity, $L_{\lambda,k}, k = 1, 2, \ldots, M$, are the spectral radiance values of the thermal radiation emitted by the cavity wall at the points of successive reflections for the corresponding temperatures $T_k, k = 1, 2, \ldots, M$.

The value of the temperature at a point of successive reflection can be computed by interpolation between the nodes. The following time-saving technique was applied. The spectral radiance values for a given set of discrete wavelengths were computed simultaneously. For each reflection, the spectral radiance of a ray was computed for every wavelength from this set, for which purpose the corresponding set of spectral reflectances for these wavelengths was assigned to the cavity surface. In other words, the same ensemble of trajectories was used for all wavelengths.

The algorithm used for non-isothermal cavities to determine the type (specular or diffuse) and direction of reflection is the same as was used for the isothermal case. Unlike in the isothermal cavity case, it is impossible to specify a criterion of ray truncation common for all cavities and all temperature distributions. Hence backward tracing of a ray ends only if this ray escapes the cavity through its aperture. The ray tracing is repeated N times, where N is a sufficiently large number of random trajectories.

We can write the estimates for the total and spectral effective emissivities of a non-isothermal cavity in the form

$$\varepsilon_{\mathrm{e,t}}(T_{\mathrm{ref}}) = \frac{\varepsilon_{\mathrm{t}}}{N T_{\mathrm{ref}}^4} \sum_{i=1}^{N} \sum_{k=1}^{M_i} \rho^{k-1} T_k^4 \qquad (12)$$

and

$$\varepsilon_{\mathrm{e},\lambda}(\lambda, T_{\mathrm{ref}}) = \frac{\varepsilon}{N}\left(\exp\left(\frac{c_2}{\lambda T_{\mathrm{ref}}}\right) - 1\right) \times \sum_{i=1}^{N} \sum_{k=1}^{M_i} \frac{\rho^{k-1}}{\exp(c_2/\lambda T_k) - 1}, \qquad (13)$$

where M_i is the number of reflections in the ith trajectory.

5. Initial data for modelling

We consider a cylindrical cavity with an inclined flat bottom. In order to reduce the number of geometrical parameters, we restrict our analysis to a cavity without a diaphragm and assume that its radius $R_{\mathrm{c}} = 1$ throughout this paper. The cavity's complete length is H as shown in figure 1. The inclined bottom extends from $z_{\min}$ to $-z_{\min}$. We considered the following parametric family of one-dimensional temperature distributions:

$$T(z) = \begin{cases} T_{\mathrm{b}}, & \text{if } z_{\min} \leqslant z \leqslant z_{\mathrm{b}}, \\ T_{\mathrm{b}} + \dfrac{T_{\mathrm{b}} - T_{\mathrm{a}}}{z_{\mathrm{b}} - z_{\max}}(z - z_{\mathrm{b}}), & \text{if } z_{\mathrm{b}} < z \leqslant z_{\max}, \end{cases} \qquad (14)$$

where z_{b} is a parameter. We assumed $T_{\mathrm{b}} \geqslant T_{\mathrm{a}}$, because the temperature in real-world cavity radiators, of the shape

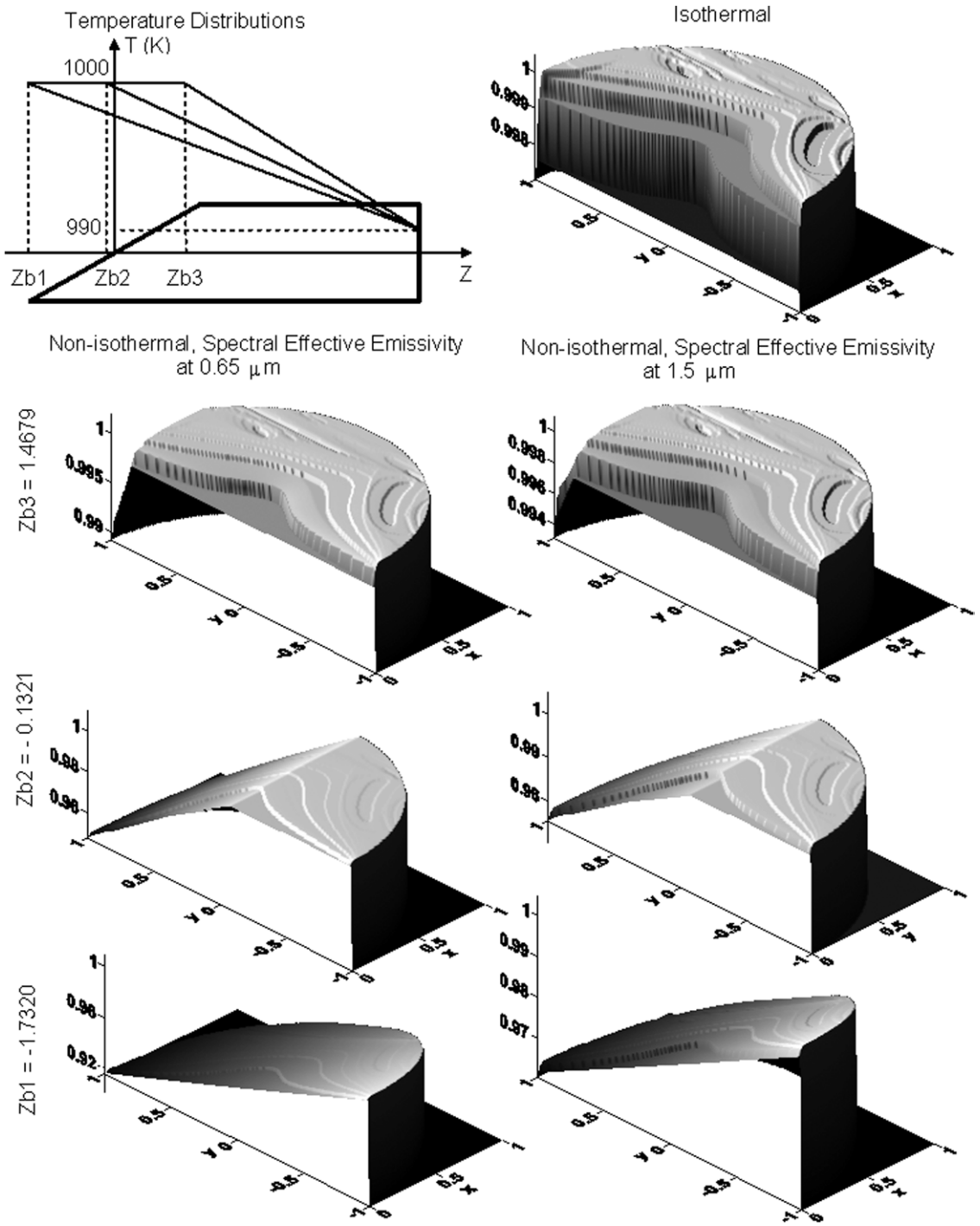

Figure 2. Distributions of the local normal effective emissivity over the aperture of a cavity with $R_c = 1$, $H = 8$, $\beta = 30^\circ$, $\varepsilon = 0.7$ and $D = 0$. The top right plot is for an isothermal cavity; the lower plots are for the non-isothermal cavity: left-hand column is for $\lambda = 0.65\,\mu$m and right-hand column is for $\lambda = 1.5\,\mu$m. $T_a = 1000$ K, $T_b = 990$ K, $T_{bg} = 0$ K. The results for three values of z_b are arranged into three rows. Due to symmetry, only the right-hand halves of the distributions are shown. The top left plot shows the temperature distributions used.

considered, typically decreases towards the aperture due to an increase in the radiative and convective heat loss in proximity to the opening. The cavity is isothermal if $z_b = z_{max}$.

The cavity radiating surface is assumed to be spatially uniform and grey (having wavelength-independent optical properties). As in the first part of this work [1], we use the uniform specular–diffuse model of reflection, which presumes that (i) the surface emits diffusely (according to Lambert's law), with an emissivity ε (for a grey surface, $\varepsilon(\lambda) = \varepsilon_t = \varepsilon$ and $\rho(\lambda) = \rho$); (ii) the directional-hemispherical reflectance $\rho = 1 - \varepsilon$ does not depend on the incidence angle and is a sum of two components—specular ρ_s and diffuse ρ_d; (iii) the diffusity of a surface, defined as $D = \rho_d/\rho$, does not depend on the incidence angle.

We also assume the validity of the ray optics approximation, no diffraction effects and full depolarization of the optical radiation due to multiple reflections inside a cavity.

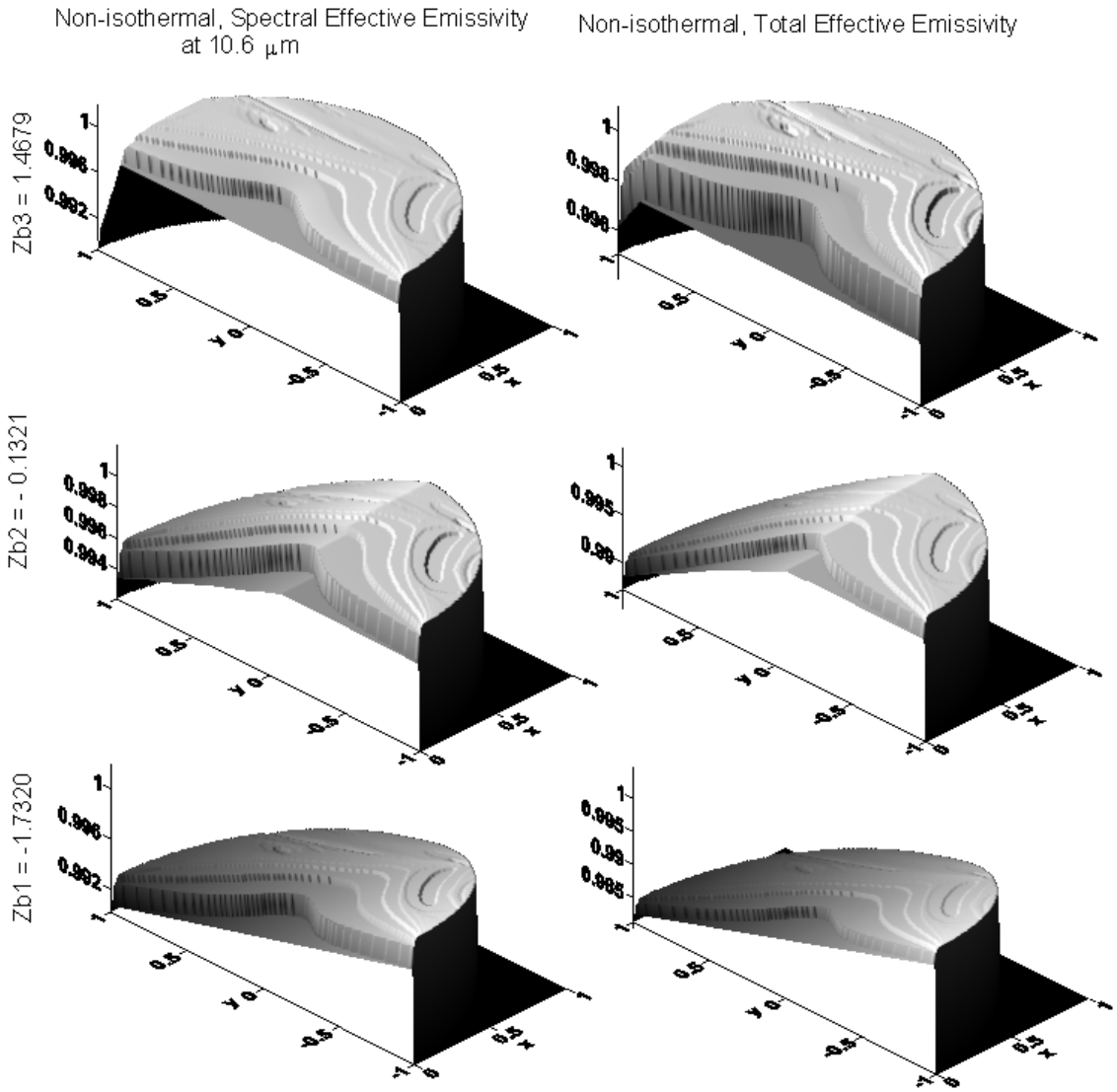

Figure 3. Distributions of the local normal effective emissivity over the aperture of a cavity with $R_c = 1$, $H = 8$, $\beta = 30^\circ$, $\varepsilon = 0.7$ and $D = 0$. $T_a = 1000\,\mathrm{K}$, $T_b = 990\,\mathrm{K}$, $T_{bg} = 0\,\mathrm{K}$. The left-hand column is for the spectral effective emissivity at $\lambda = 10.6\,\mu\mathrm{m}$ and the right-hand column is for total effective emissivity. The results for three values of z_b are arranged into three rows.

6. Distribution of the local normal effective emissivity

It was shown in the first part of this work [1] that the distribution of the local normal effective emissivity over the aperture of an isothermal cavity with an inclined bottom and purely specular walls is non-uniform but forms zones of complicated shapes. The diffuse component of reflection smoothes this non-uniformity. The influence of the temperature non-uniformity on the distribution of the normal effective emissivity for a purely specular ($D = 0$) cavity with $H = 8$, $\beta = 30^\circ$ and an emissivity of its internal surface $\varepsilon = 0.7$ is shown in figure 2 and figure 3 for $T_{ref} = T_b = 1000\,\mathrm{K}$, $T_a = 990\,\mathrm{K}$ and $T_{bg} = 0\,\mathrm{K}$.

The temperature distributions used for calculations are shown at the top left of figure 2. A three-dimensional view of the local normal effective emissivity distribution for isothermal cavity ($z_b = z_{max} = 6.2679$) is depicted at the top right. In the same figure, the distributions of the normal spectral effective emissivity for three values of z_b (-1.7320, 0.1321 and 1.4679) and two wavelengths ($0.65\,\mu\mathrm{m}$ and $1.5\,\mu\mathrm{m}$) are arranged in rows and columns, respectively. Distributions of the normal spectral effective emissivity at $10.6\,\mu\mathrm{m}$ and of the total normal effective emissivity for the same values of z_b are arranged in the same manner in figure 3. For the cavity with the geometrical parameters specified above, $z_{min} = -1.7320$. All the three above-mentioned values of z_b belong to the interval $[z_{min}, -z_{min}]$. The temperature non-uniformity of a part of this interval (i.e. of the part of a cavity bottom) leads to a near-linear decrease in the local normal effective emissivity on this part. In comparison with this decrease, the relief of the local normal effective emissivity distribution on the isothermal part of the bottom becomes imperceptible. When $z_b \notin [z_{min}, -z_{min}]$, the influence of the temperature non-uniformity is practically unobservable. This is due to the fact that, for a cavity with $\beta = 30^\circ$, for all incoming rays that are

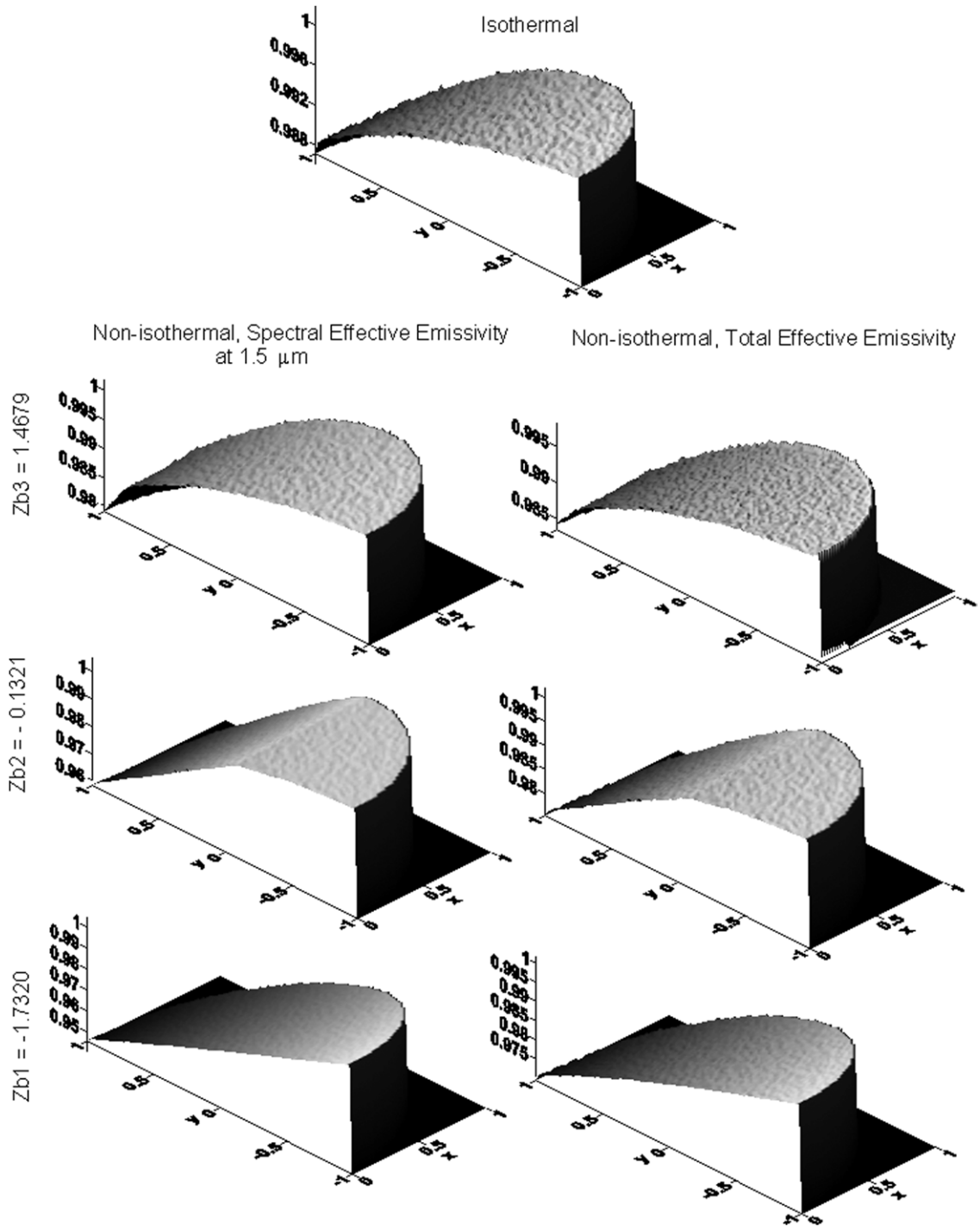

Figure 4. Distributions of the local normal effective emissivity over the aperture of a cavity with $R_c = 1$, $H = 8$, $\beta = 30^\circ$, $\varepsilon = 0.7$ and $D = 1$. $T_a = 1000\,\mathrm{K}$, $T_b = 990\,\mathrm{K}$, $T_{bg} = 0\,\mathrm{K}$. The top plot is for the isothermal cavity. Below, the left-hand column is for the spectral effective emissivity at $\lambda = 1.5\,\mu\mathrm{m}$ and the right-hand column is for the total effective emissivity. The results for three values of z_b are arranged into three rows.

parallel to the cavity axis, after first reflection from the inclined bottom the points of all further reflections are contained within the interval $[z_{min}, -z_{min}]$.

For a diffuse cavity with the same parameters, the behaviour is different. The influence of temperature non-uniformity on the distribution of the normal effective emissivity for a purely diffuse ($D = 1$) cavity with $H = 8$, $\beta = 30^\circ$ and an emissivity of its internal surface $\varepsilon = 0.7$, is shown in figure 4 for $T_{ref} = T_b = 1000\,\mathrm{K}$, $T_a = 990\,\mathrm{K}$ and $T_{bg} = 0\,\mathrm{K}$. A three-dimensional view of the distribution for an isothermal diffuse cavity ($z_b = z_{max} = 6.2679$) is depicted at the top of figure 4. This distribution was computed at the nodes of a 101×201 rectangular grid, which lie inside a unit half-circle. For every node, 10^5 rays were traced. The apparent 'roughness' of a plotted surface that represents the effective emissivity distribution is a result of the random uncertainty of

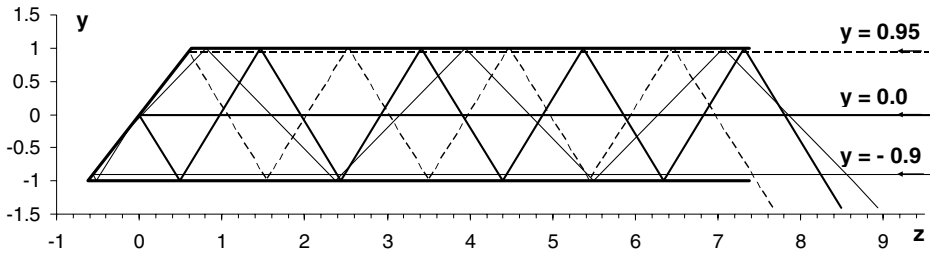

Figure 5. Backward ray tracing in a cavity with $R_c = R_a = 1$, $H = 8$, $\beta = 58^\circ$ and $D = 0$, performed for three rays that lie on the cavity's plane of symmetry.

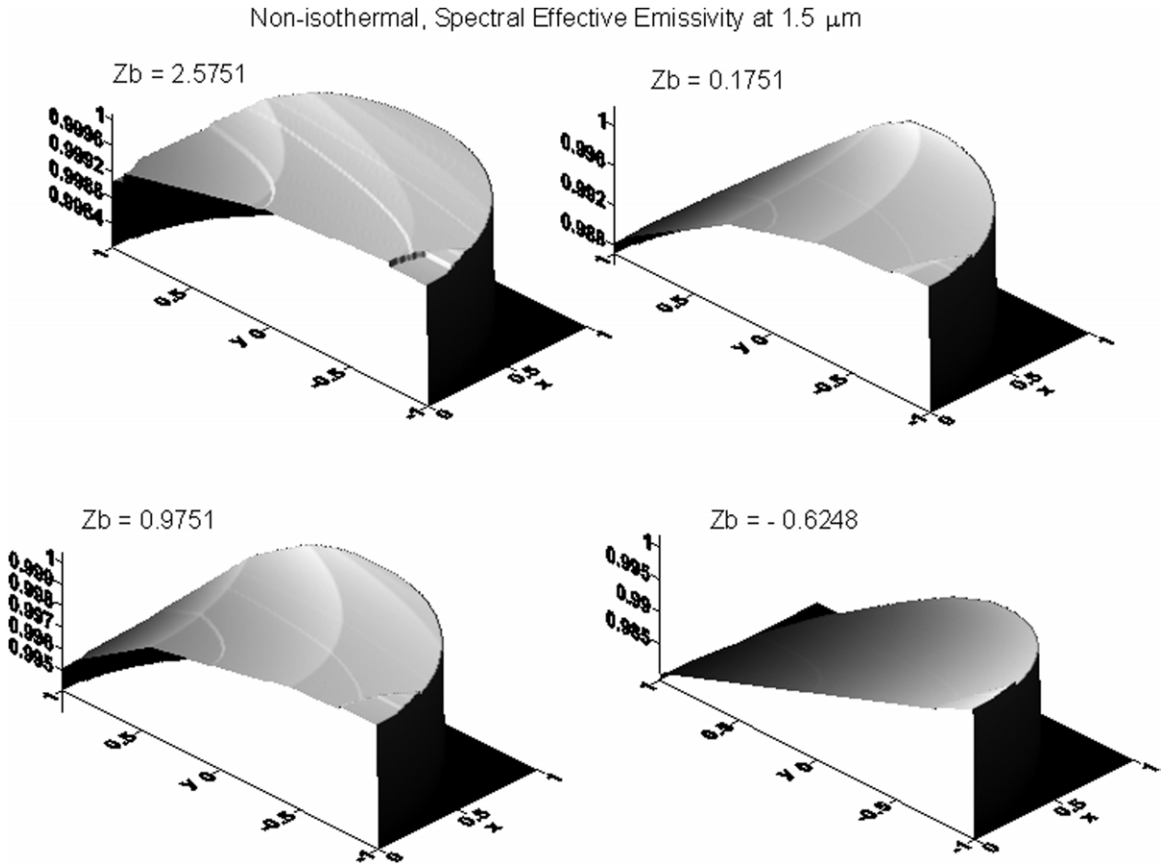

Figure 6. Distributions of the local normal spectral effective emissivity at $\lambda = 1.5\,\mu\text{m}$ for a cavity with $R_c = 1$, $H = 8$, $\beta = 58^\circ$, $\varepsilon = 0.7$, $D = 0$ and four values of z_b. $T_a = 1000\,\text{K}$, $T_b = 990\,\text{K}$, $T_{bg} = 0\,\text{K}$.

the stochastic method with a standard deviation $s = 2 \times 10^{-5}$. In general, the value of s varies from almost 0 for a purely specular cavity (this is the case of deterministic reflections; the random uncertainty is associated only with the Monte Carlo integration over the aperture) to 3×10^{-4} for a 'nearly' black specular–diffuse cavity (having an effective emissivity of about 0.99). The distributions of the normal spectral effective emissivity at 1.5 μm and of the total normal effective emissivity for three values of z_b (-1.7320, 0.1321 and 1.4679) are shown in figure 4. When the cavity's bottom is isothermal ($z_b \geqslant 1.7320$), the distribution's shape is minimally affected by the cylindrical section's temperature non-uniformity, but the span of the distribution's non-uniformity slightly decreases as z_b increases. The linear temperature drop along the part of the inclined bottom leads to an almost linear decrease in effective emissivity on the bottom's non-isothermal part.

For the purely specular cavity with $H = 8$ and $\beta = 58^\circ$, the points of consecutive reflections are distributed along the cylindrical wall. The inverse ray tracing of three rays that lie in the cavity's plane of symmetry is displayed in figure 5.

The plots in figure 6 present the distributions of the normal spectral effective emissivity at 1.5 μm of a non-isothermal specular ($D = 0$) cavity with $H = 8$, $\beta = 58^\circ$ and an emissivity of the internal surface $\varepsilon = 0.7$. The cavity with these geometrical parameters has $z_{min} = -0.6249$. Thus $z_b = 0.1751$, 0.9751 and 2.5751 correspond to the cases of an isothermal bottom. However, even for these values of z_b, the temperature non-uniformity of the cylindrical wall distorts the normal effective emissivity distributions. This appears as a series of overlapped areas, in which the effective emissivity decreases continuously. Every area has its own slope that corresponds to a certain number of consecutive reflections.

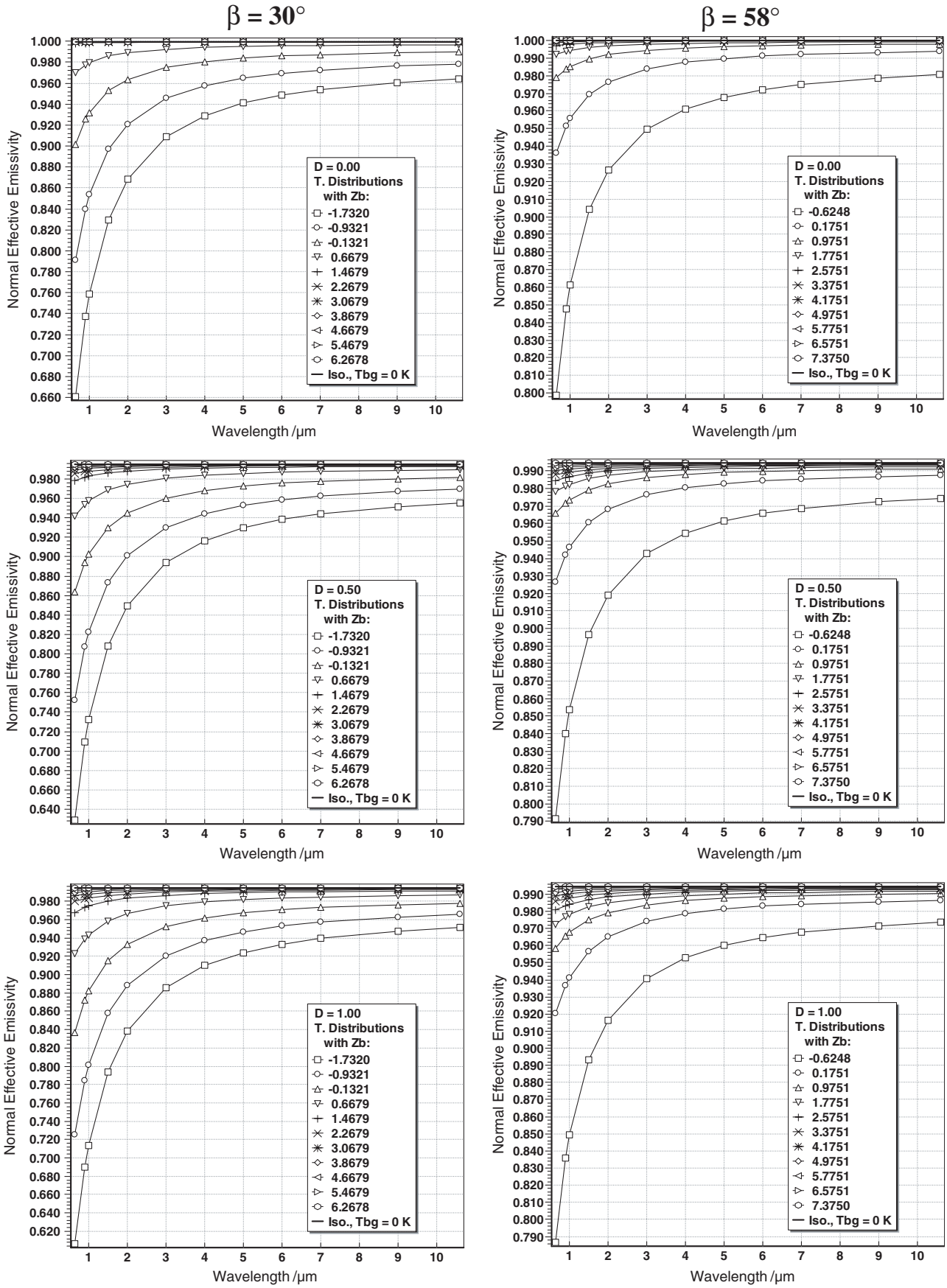

Figure 7. Average normal spectral effective emissivity of two cavities with $R_c = 1$, $H = 8$ and $\varepsilon = 0.7$; $\beta = 30^\circ$ and 58°, for $D = 0$, 0.5 and 1, for several values of z_b. $T_{ref} = T_b = 1000\,\mathrm{K}$, $T_a = 990\,\mathrm{K}$ and $T_{bg} = 0\,\mathrm{K}$.

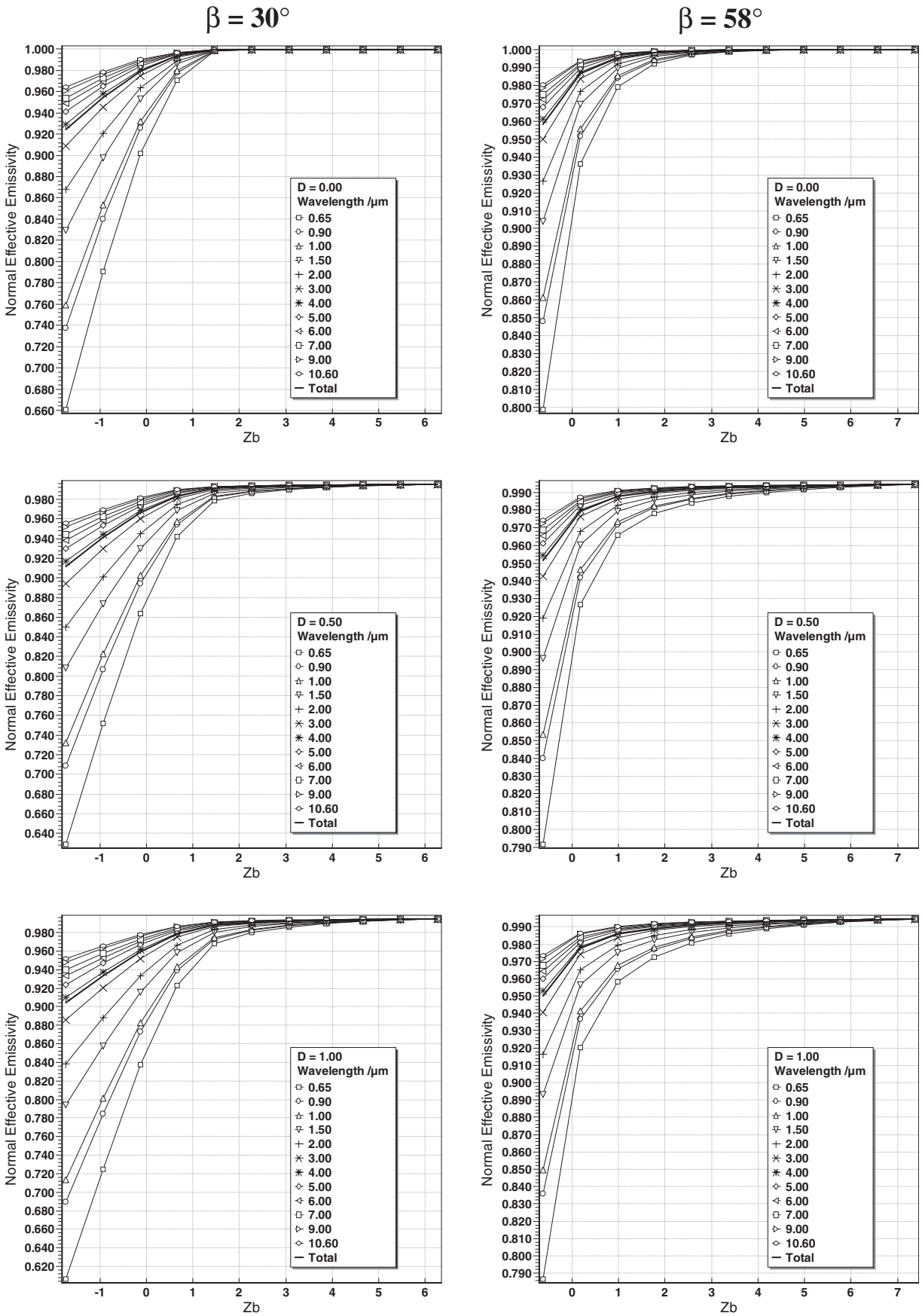

Figure 8. Average normal spectral effective emissivity as a function of z_b for two cavities with $R_c = 1$, $H = 8$, and $\varepsilon = 0.7$; $\beta = 30^\circ$ and 58°, for $D = 0$, 0.5 and 1, for several values of λ; $T_{ref} = T_b = 1000\,K$, $T_a = 990\,K$ and $T_{bg} = 0\,K$.

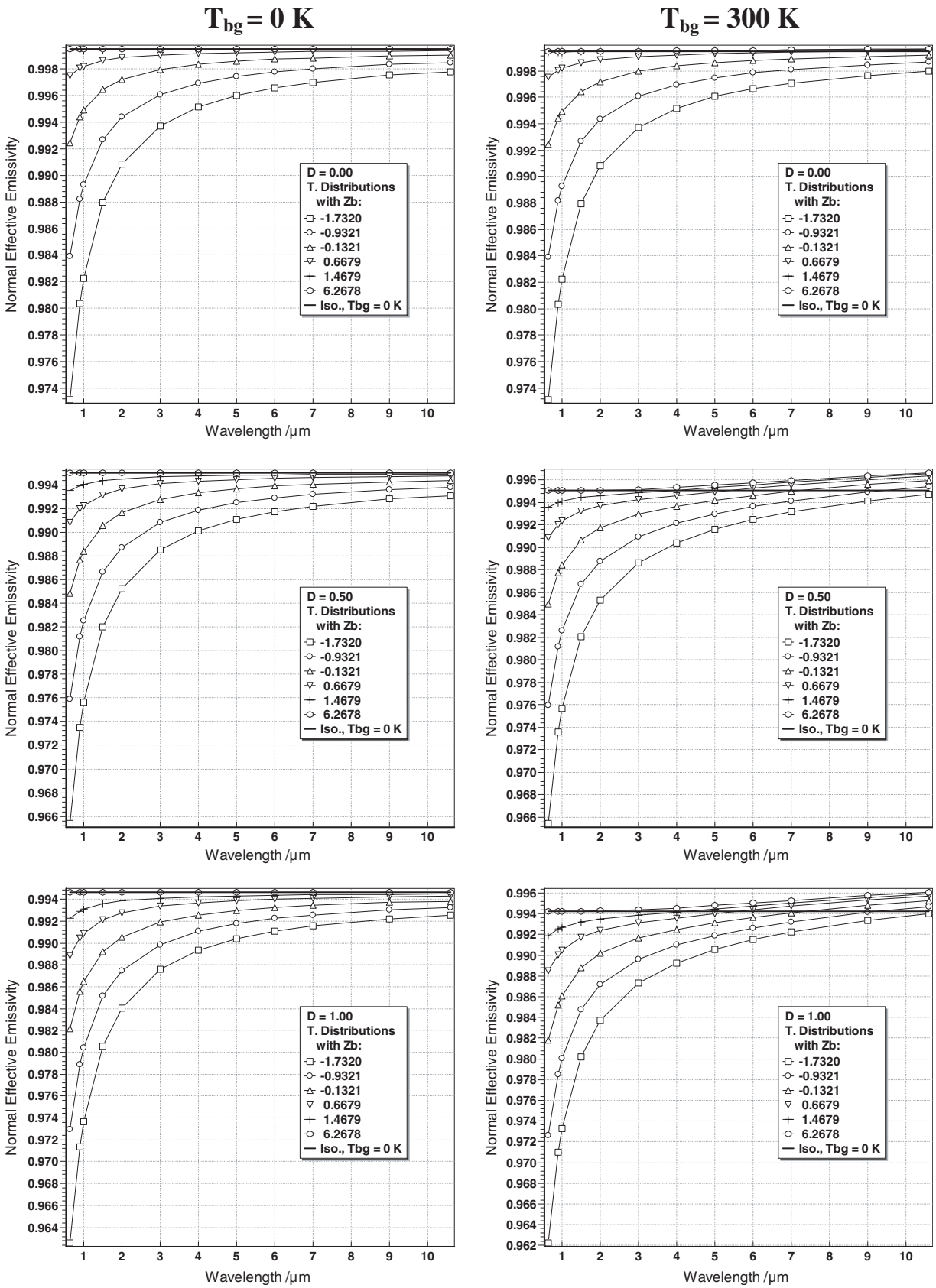

Figure 9. Average normal spectral effective emissivity of a cavity with $R_c = 1$, $\beta = 30^\circ$, $H = 8$ and $\varepsilon = 0.7$, for $D = 0$, 0.5 and 1, for several values of z_b; $T_{ref} = T_b = 400\,\mathrm{K}$, $T_a = 399\,\mathrm{K}$, $T_{bg} = 0\,\mathrm{K}$ and $T_{bg} = 300\,\mathrm{K}$.

If nearly the entire bottom becomes non-isothermal ($z_b = -0.6248$), the distribution looks like an inclined plane, the slope of which is primarily determined by the non-uniformity of the bottom temperature.

The results, presented in figures 2–4 and 6, show that the non-uniformity of the local effective emissivity distribution decreases as the wavelength increases. The total effective emissivity has an in-between value, nearer to that for the long-wave edge of the spectral range considered.

7. Average normal effective emissivity

We modelled the average normal effective emissivity by inverse tracing of the rays that are parallel to the cavity axis and uniformly distributed over the aperture. The computed dependences of the normal spectral effective emissivity on wavelength for two cavities with the bottom inclination angles of 30° and 58° are shown in figure 7. The other parameters of both cavities are $H = 8, \varepsilon = 0.7$. The results presented in figure 7 are obtained for $D = 0$, 0.5 and 1 and for 11 values of z_b, uniformly distributed on the interval $[z_{min}, z_{max}]$. The thick solid lines are for the corresponding isothermal cavity and non-emitting environment cases. The drop in the normal spectral effective emissivity in the short-wave spectral range for a cavity with $\beta = 30°$ is greater than that for a cavity with $\beta = 58°$ because the extent of its bottom in the z-direction is greater, and this leads to a greater temperature non-uniformity of its projection onto the plane that is normal to the cavity axis. However, in the case of $D = 0$, the curves for a cavity having $\beta = 30°$ coincide with the line for the isothermal cavity as soon as z_b becomes greater than $-z_{min}$ because all the points of reflection are concentrated in the interval $[z_{min}, -z_{min}]$. The curves of the normal spectral effective emissivity for both cavities become asymptotic to that of the isothermal cavity when the wavelength increases.

The same data are presented in figure 8 as a function of z_b, with the wavelength as a parameter of the family of curves. These dependences are homomorphous but differ in their numerical value.

In order to check equation (9), we performed a direct simulation of the influence of the radiating environment. For this purpose, we considered the backward traced ray that left a cavity as an incident ray having the spectral radiance computed by Planck's equation for the given wavelengths and for the background temperature T_{bg}. We obtained very good agreement with the effective emissivities computed using equation (9).

For comparison, the results of the modelling for $T_{ref} = T_b = 400\,K$, $T_a = 399\,K$; $T_{bg} = 0\,K$ and $T_{bg} = 300\,K$ are arranged in two columns in figure 9. The influence of the background temperature on a purely specular cavity with $\beta = 30°$ is minimal because the backward traced ray undergoes at least five reflections until it escapes a cavity. Thus, its initial radiance will be multiplied by ρ^5 (or smaller). The diffuse component of reflection allows some of the rays to leave the cavity through its aperture after each reflection. This leads to the increase in the normal spectral effective emissivity in the long-wave range, so its value can exceed the level of the normal effective emissivity of the isothermal cavity computed for $T_{bg} = 0\,K$. Let us consider the function

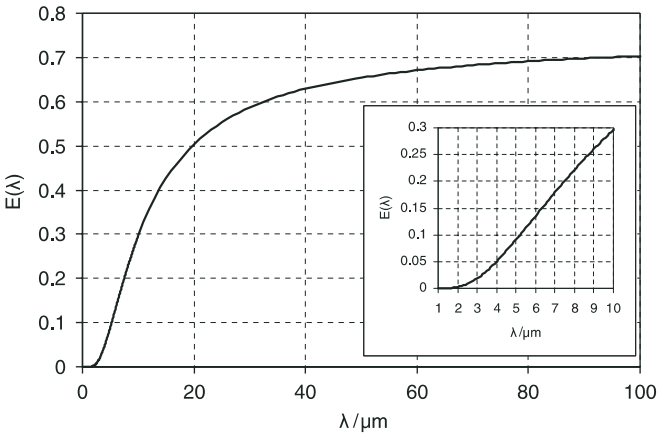

Figure 10. Plot of the function $E(\lambda)$ defined by equation (10).

$$E(\lambda) = \frac{\exp(c_2/\lambda T_{ref}) - 1}{\exp(c_2/\lambda T_{bg}) - 1}. \qquad (15)$$

The plot of the function $E(\lambda)$ is shown in figure 10 for $T_{ref} = 400\,K$ and $T_{bg} = 300\,K$. The graph of $E(\lambda)$ grows linearly in the spectral range from about 4 μm to approximately 10 μm. This explains the nearly linear increase in the spectral effective emissivity in this wavelength range in the plots of the right-hand column in figure 9.

8. Hemispherical effective emissivity

To simulate the uniform hemispherical irradiation of the cavity opening, which is necessary for backward ray tracing, we closed the cavity opening with a virtual black disc that is a Lambertian source of initial rays but has zero temperature. We considered cavities with $H = 8, \beta = 30°, \varepsilon = 0.7$; $T_{ref} = 1000\,K$, $T_{bg} = 0\,K$, $T_b = 1000\,K$ and $T_a = 990\,K$. The left-hand column in figure 11 shows the dependences of the hemispherical spectral effective emissivity on wavelength for three values of the diffusity D and several values of the parameter z_b of the temperature distributions family. The right-hand column in figure 11 displays the dependences of the hemispherical spectral effective emissivity on z_b for three values of D and several wavelengths. These plots can be compared with those in the left-hand columns in figures 7 and 8 for the normal effective emissivity of the same cavity. One can see that the values of the hemispherical effective emissivity are always lower than the corresponding values of the normal effective emissivity. Hemispherical values are more sensitive to the temperature non-uniformity than the normal ones. For the same cavity but with $\beta = 58°$, the curves of the hemispherical effective emissivity were also obtained. They are qualitatively similar to the curves for the $\beta = 30°$ case and differ only in their numerical values.

9. Practical application

In order to demonstrate the practical application of the algorithm and computer code developed, we computed the

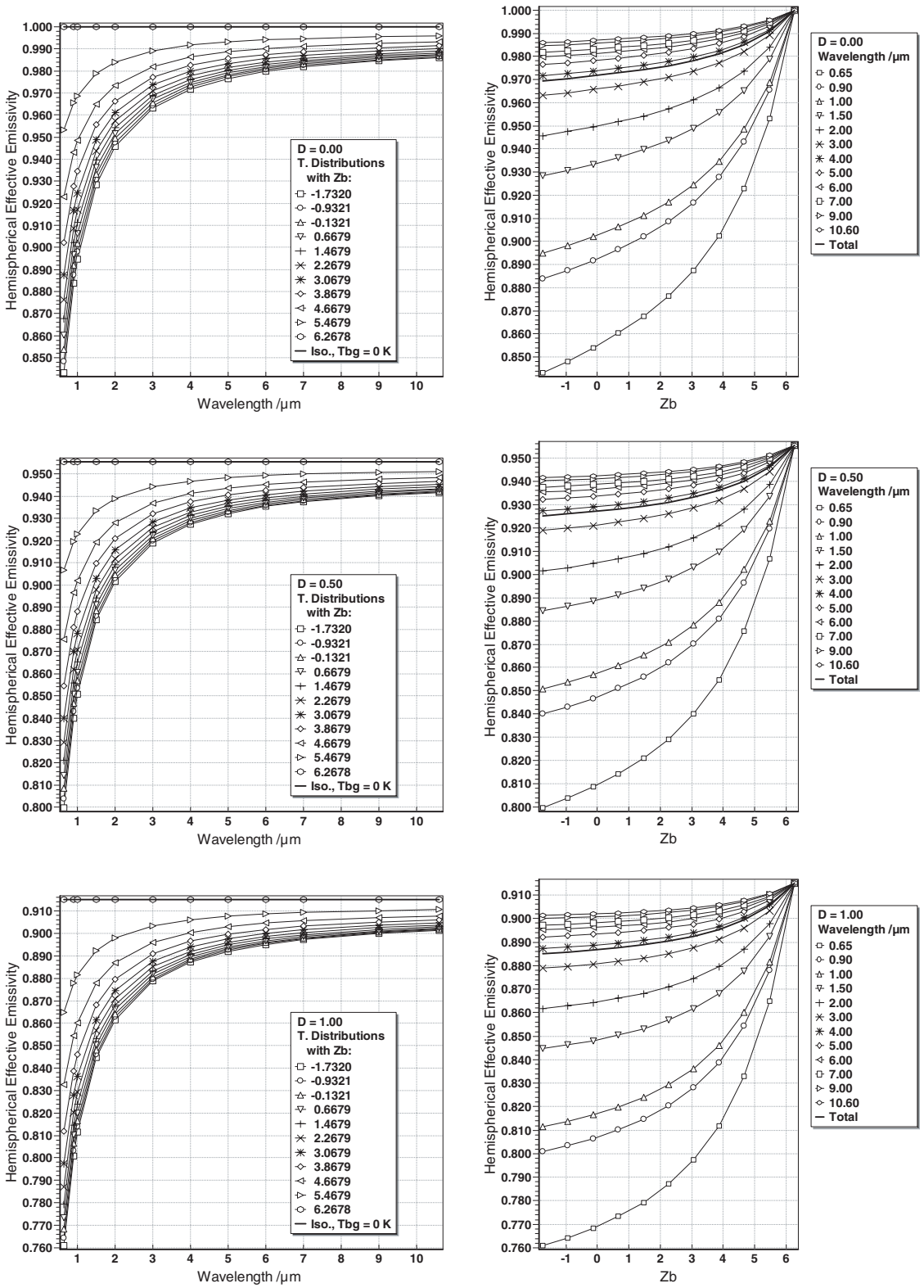

Figure 11. Hemispherical effective emissivities of the cavity with $R_c = 1$, $\beta = 30^\circ$, $H = 8$ and $\varepsilon = 0.7$, for $D = 0$, 0.5 and 1; $T_{ref} = T_b = 1000\,K$, $T_a = 990\,K$ and $T_{bg} = 0\,K$. In the left-hand column: dependences on λ for several values of z_b. In the right-hand column: dependences on z_b for several values of λ.

effective emissivity of a cavity which is recommended by the European standard on clinical thermometers as an 'example for suitable design of a black body radiator' [7] for the testing of clinical infrared ear thermometers. This cavity is a cylinder with an inclined flat bottom and a flat diaphragm. The parameters of the cavity are the following: $R_c = 19.5\,mm$, $R_a = 5\,mm$, $H = 105\,mm$ and $\beta = 30^\circ$. A diffusely reflecting ($D = 1$) black paint of spectral emissivity greater than 0.95 in the wavelength range from 8 μm to 15 μm is recommended for the cavity's internal surface coating. The

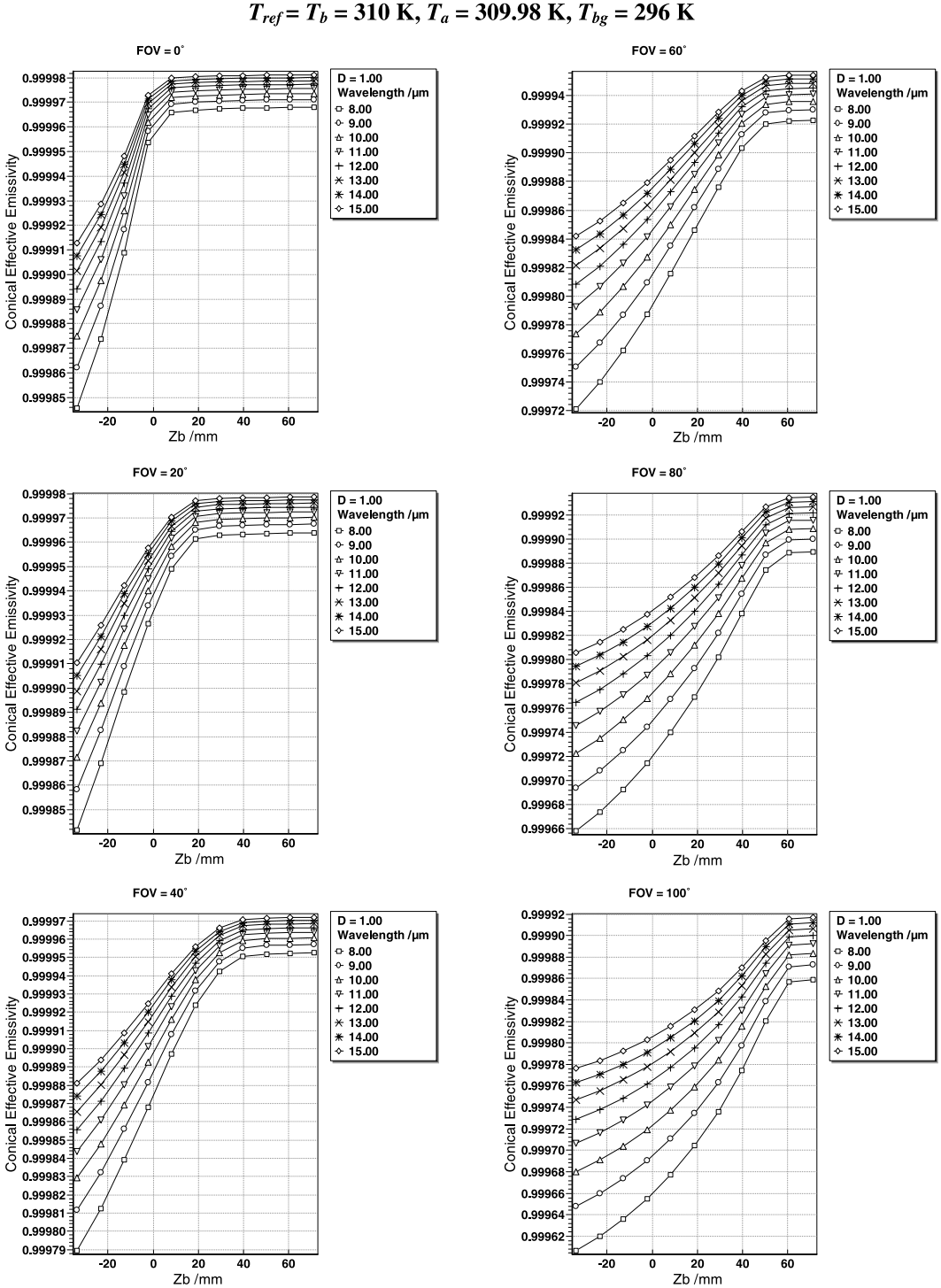

Figure 12. Conical spectral effective emissivities of the blackbody for calibration of the infrared ear thermometers as a function of z_b for six values of the conical FOV apex angle: 0°, 20°, 40°, 60°, 80° and 100°. Blackbody cavity parameters are conformed to the European Standard [7]: $R_c = 19.5$ mm, $R_a = 5$ mm, $H = 105$ mm and $\beta = 30°$; $\varepsilon(\lambda) = 0.95$ for 8 μm $< \lambda <$ 15 μm, $D = 1$. $T_{ref} = T_b = 310$ K, $T_a = 309.98$ K, $T_{bg} = 296$ K.

radiating cavity is immersed in a water bath at temperatures from 15 °C to 45 °C. Even if we consider the water inside the bath isothermal and eliminate convective heat transfer from the cavity's internal surface, it will be non-isothermal due to the difference in radiation heat losses of areas at different distances from the cavity's aperture. We adopted the value of 20 mK for the temperature non-uniformity that was used in [8]. However, differently from [8], we used the family of temperature distributions in the form represented by equation (14) with the parameter z_b instead of the linear temperature distribution that was used in [8]. The other initial data were the following: $T_{ref} = T_b = 310$ K, $T_a = 309.98$, $T_{bg} = 296$ K. According to [7], the calibration of the ear thermometer is performed by the insertion of its probe end

into the aperture opening of the cavity. Different types of ear thermometers have different angular fields-of-view (FOVs). In order to evaluate the effect of FOV on the effective emissivity of a non-isothermal cavity, we performed the modelling for various FOVs from 0° to 100°. We assumed that the base radius of a conical FOV coincides with the aperture radius. Since we had no data on the ear thermometer's probe end emissivity, we assumed that the probe end radiates as a perfect blackbody at the background temperature T_{bg}. If the sensor's emissivity is known, the corrections for it and for the radiation heat exchange between the sensor and the cavity can be computed as this was done in [9]. A part of the computed dependences of the conical spectral effective emissivities on z_b is presented in figure 12 for six values of the conical FOV apex angles. Each plot was obtained by tracing 10^6 rays. The absolute standard deviation of random uncertainty in the determination of effective emissivity is less than 5×10^{-6}.

The first plot in figure 12 corresponds to the normal effective emissivities averaged over the cavity aperture (FOV = 0°). All of the plots presented in figure 12 show that due to the low value of cavity's wall reflectance ($\rho = 0.05$), the effective emissivity is only slightly affected by the temperature non-uniformity of a cavity portion that is out of FOV. The right-hand edges correspond to the isothermal cavity at 310 K. The left-hand edges correspond to a linear temperature decrease from 310 K to 309.98 K towards the cavity opening.

The spectral emissivities at shorter wavelengths are more sensitive to the temperature variations than those at longer wavelengths. In figure 12, the maximal difference in the conical effective emissivity (0.999 82 for FOV = 0° and 0.999 61 for FOV = 100°) corresponds to the wavelength of 8 µm and entirely non-isothermal cavity. Elementary calculations show that such a difference in effective emissivity leads to a difference in radiance temperatures at 8 µm of about 10 mK.

10. Conclusion

We have considered some features of non-isothermal specular cavities with an inclined bottom. Our analysis has been performed in the framework of ray optics and the specular–diffuse model of reflection. The Monte Carlo algorithm that uses backward ray tracing is applied to non-isothermal cavities whose one-dimensional temperature fields were modelled using a one-parameter piecewise-linear family of distributions.

The distributions of the spectral and total local normal effective emissivity over the cavity aperture were calculated and the results were analysed. It is shown that the extent to which the distribution of local normal effective emissivity is affected by the temperature non-uniformity of the cylindrical part of a cavity is considerably determined by the diffusity of its wall and the bottom inclination angle.

The average normal and hemispherical effective emissivities were computed as functions of the wavelength and the parameter z_b of a family of the temperature distributions. The effect of background temperature on the cavity's effective emissivity is evaluated.

As a practical example, the dependences of the effective emissivities on the apex angle of the conical FOV of the radiation thermometer were calculated for a blackbody cavity which has parameters recommended by the European Standard [7] for the calibration of infrared ear thermometers.

It should be remembered that polarization can play an important role in the radiation transfer inside the cavity, especially with specularly reflecting walls. Unlike an axially symmetric cavity, a cavity with an inclined bottom has no axial symmetry; the polarization of the emitted and reflected radiation could be incompletely suppressed after multiple reflections, so that the exiting radiation could be polarized. In addition, it should be noted that the specular–diffuse model of reflection is no more than a simple and convenient approximation of the real angular characteristics of the reflected radiation. The radiation characteristics of a cavity with an inclined bottom and real optical properties of the cavity wall require further study.

References

[1] Prokhorov A V and Hanssen L M 2004 *Metrologia* **41** 421–31
Prokhorov A V and Hanssen L M 2009 *Metrologia* **46** 719 (erratum)

[2] Bedford R E 1988 Calculation of effective emissivities of cavity sources of thermal radiation *Theory and Practice of Radiation Thermometry* ed D P DeWitt and G D Nutter (New York: Wiley) pp 653–772

[3] Prokhorov A V, Hanssen L M and Mekhontsev S N 2009 Calculation of radiation characteristics of blackbody radiation sources *Radiometric Temperature Measurements Volume 42: I. Fundamentals* (*Experimental Methods in the Physical Sciences*) ed Z Zhang *et al* (New York: Academic) pp 181–240

[4] Bedford R E and Ma C K 1974 *J. Opt. Soc. Am.* **64** 339–49

[5] Chu Z, Wang C and Li B 1987 *Appl. Opt.* **26** 207–8

[6] Mohr P J, Taylor B N and Newell D B 2008 *Rev. Mod. Phys.* **80** 633–730

[7] European Standard EN 12470-5:2003 2003 Clinical Thermometers—Part 5: Performance of Infrared Ear Thermometers (with Maximum Device) CEN TC205 23–5

[8] Ishii J, Fukuzaki T, Kojima T and Ono A 2001 *TEMPMEKO 2001: Proc. 8th Int. Symp. on Temperature and Thermal Measurements in Industry and Science (Berlin, Germany)* pp 729–34

[9] Murthy A V, Prokhorov A V and DeWitt D P 2004 *J. Thermophys. Heat Transfer* **18** 333–41